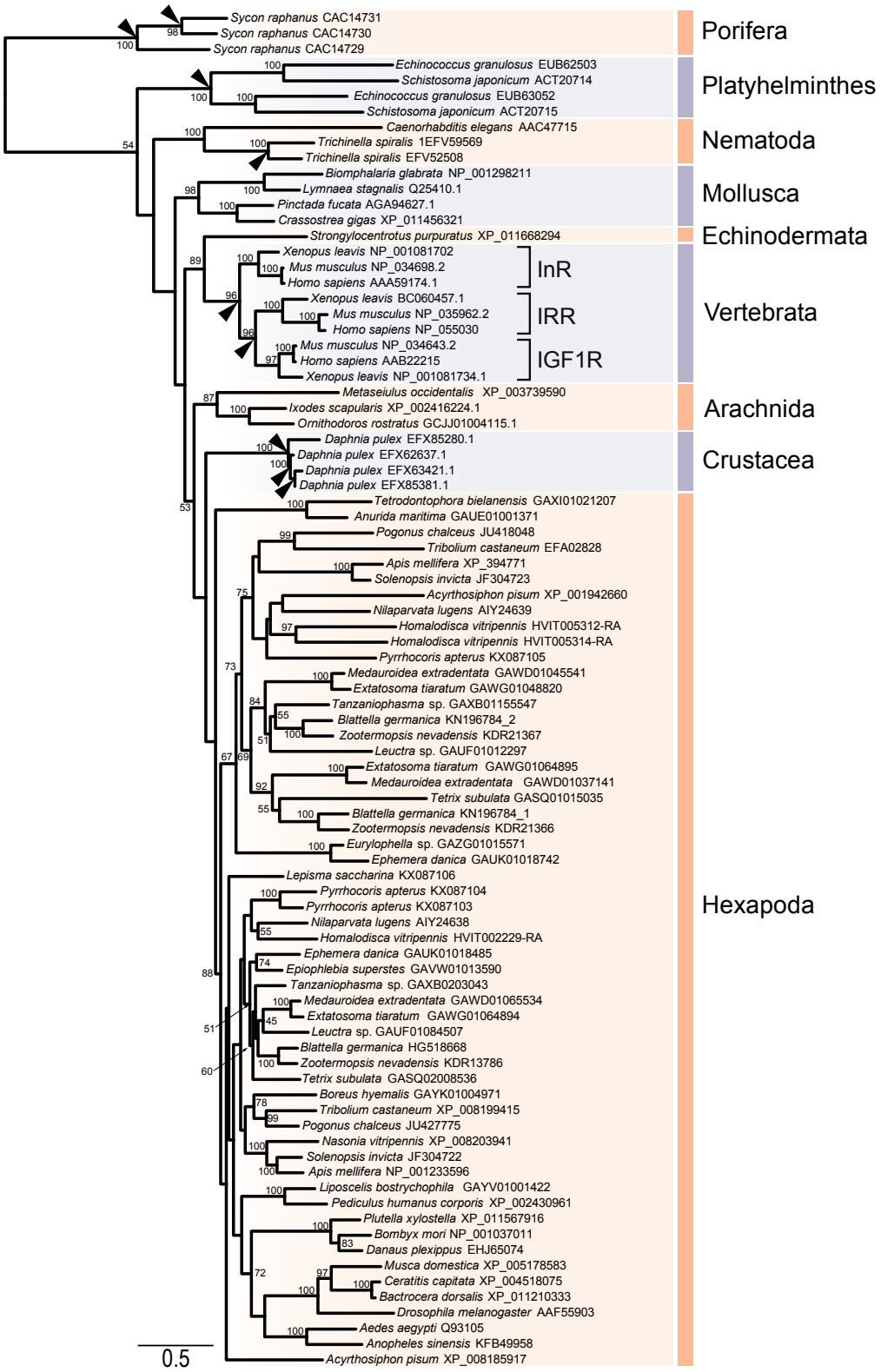

Supplementary Figure 1. Phylogenetic tree of insulin receptor protein sequences identified across Animalia, including selected representatives of Insecta. *Sycon raphanus* InR sequences were set as outgroup. Duplication events in non-insect phyla are marked with arrowheads. The topology and branching supports were inferred using RAxML maximum likelihood algorithm with WAG + Γ model (-ln = 131220.705824), the bootstrap values calculated from 1000 replicates are shown for nodes represented in more than 50% of trees. InR, insulin receptor; IRR, insulin receptor-related receptor; IGF1R, insulin-like growth factor 1 receptor.

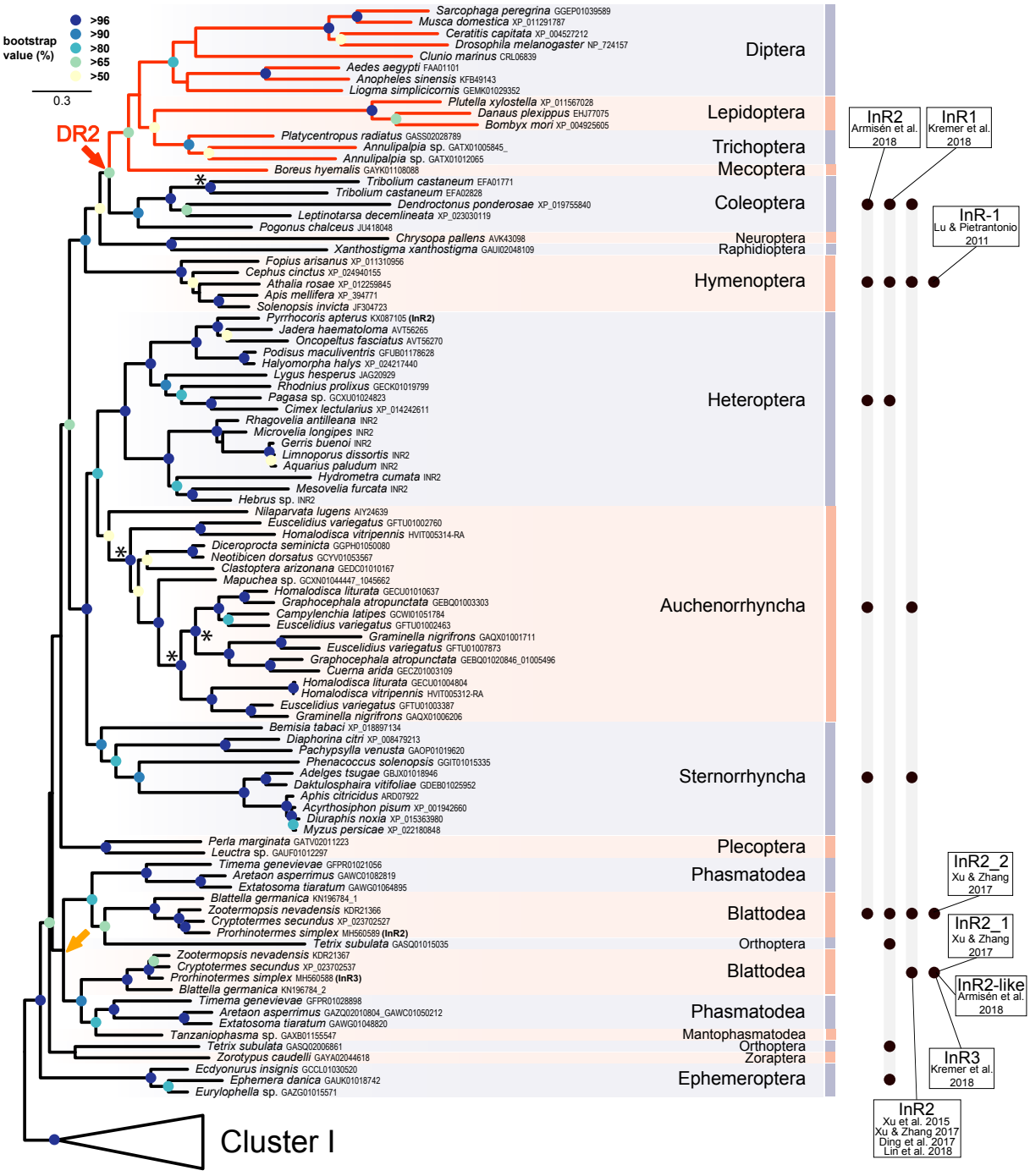

Supplementary Figure 2. Phylogenetic tree and nomenclature of insect insulin receptors and decoy of insulin receptors identified in the Cluster II in 98 species from 23 orders. The tree represents the full version of the simplified tree given in Figure 1 of the main text. Orange arrow marks the Cluster II duplication within Polyneoptera. Red arrow (DR2) marks the loss of the tyrosine kinase domain giving rise to the decoy of insulin receptor gene DR2 (red) in Mecopterida, a group of advanced Holometabola including Diptera, Lepidoptera, Trichoptera and Mecoptera. Asterisks mark the duplication identified in *Tribolium castaneum* and the multiple duplications in Auchenorrhyncha. The topology and branching supports were inferred using RAxML maximum likelihood algorithm with WAG + Γ model (-ln = 285839.374747) the bootstrap values calculated from 500 replicates are shown for nodes represented in more than 50% of trees. Black dots in the right part of the figure indicate the insect orders included in phylogenetic analyses in previous studies, the boxes give the nomenclature used by previous studies for the identified InR genes. Bold marking in brackets shows the InR nomenclature used in this study for *P. simplex* and *P. apterus* InRs.

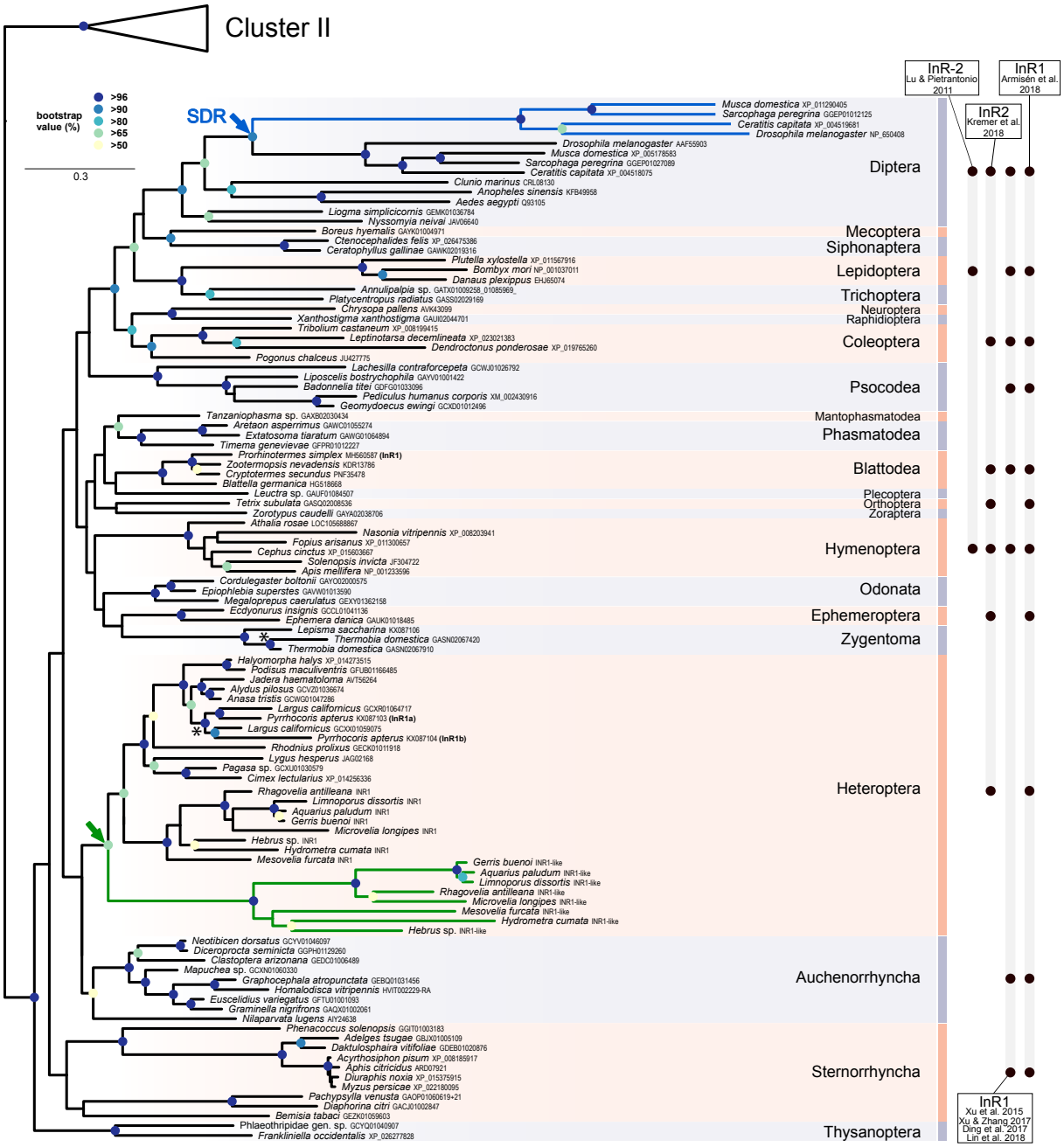

Supplementary Figure 3. Phylogenetic tree and nomenclature of insect insulin receptors and decoy of insulin receptors identified in the Cluster I in 98 species from 23 orders. The tree represents the full version of the simplified tree given in Figure 1 of the main text. Green arrow marks the Cluster I duplication in Gerromorpha, blue arrow (SDR) marks the loss of the tyrosine kinase domain in Muscomorpha, giving rise to the secreted decoy of insulin receptor gene SDR (blue). Asterisks mark the duplication identified in Pyrrhocoridae and in *Thermobia domestica*. The topology and branching supports were inferred using RAxML maximum likelihood algorithm with WAG + Γ model (-ln = 285839.374747) the bootstrap values calculated from 500 replicates are shown for nodes represented in more than 50% of trees. Black dots in the right part of the figure indicate the insect orders included in phylogenetic analyses in previous studies, the boxes give the nomenclature used by previous studies for the identified InR genes. Bold marking in brackets shows the InR nomenclature used in this study for *P. simplex* and *P. apterus* InRs.

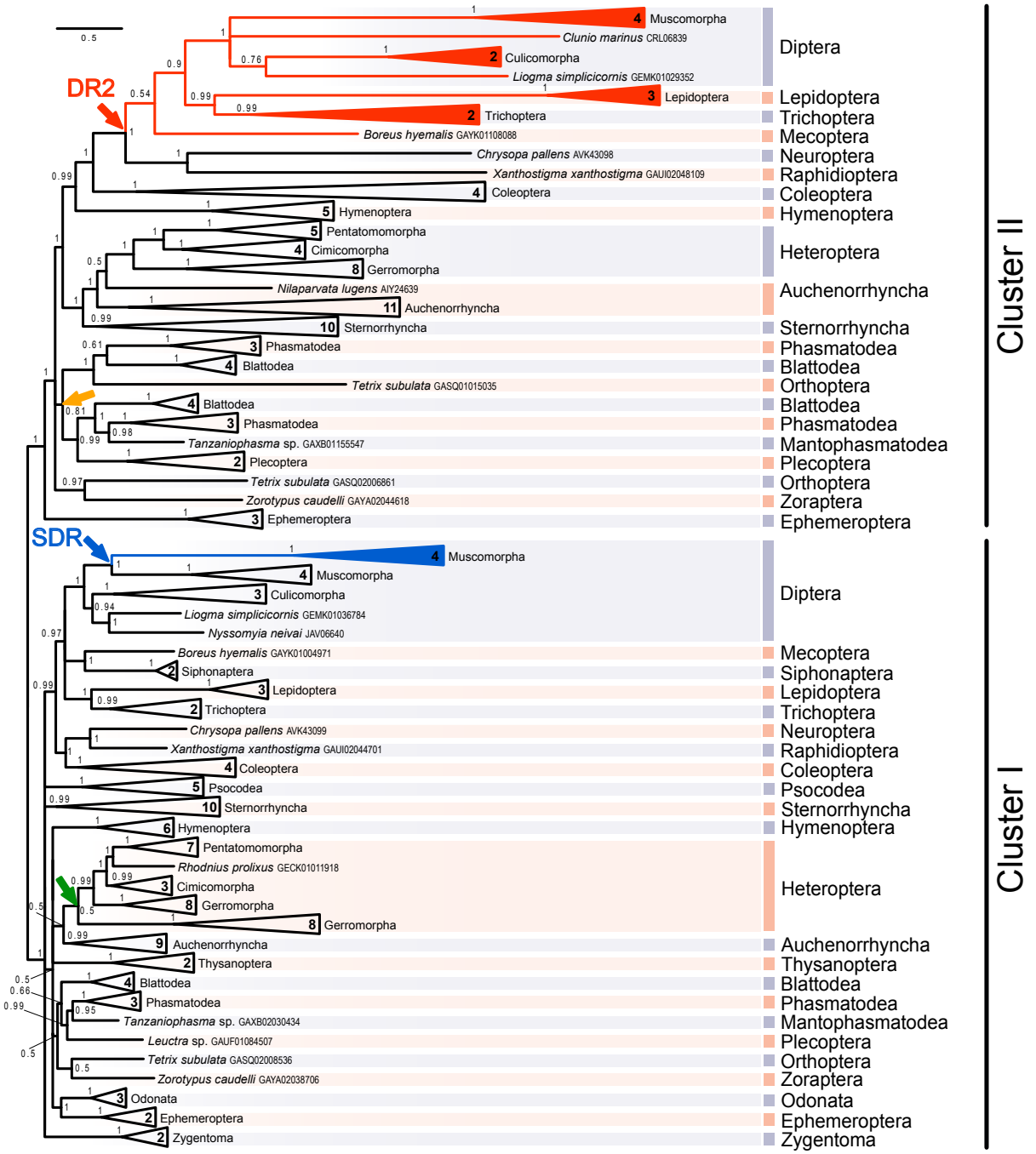

Supplementary Figure 4. Phylogenetic tree of insect insulin receptor genes and decoy of insulin receptor genes identified in 98 species from 23 orders. The numbers in condensed branches indicate the numbers of species. Orange arrow marks the Cluster II duplication within Polyneoptera, red arrow (DR2) marks the loss of the tyrosine kinase domain in advanced Holometabola, giving rise to the decoy of insulin receptor gene DR2 (red). Green arrow marks the Cluster I duplication in Gerromorpha, blue arrow (SDR) marks the loss of the tyrosine kinase domain in Muscomorpha, giving rise to the secreted decoy of insulin receptor gene SDR (blue). The topology and branching supports are based on Bayesian inference (PhyloBayes v4.1).

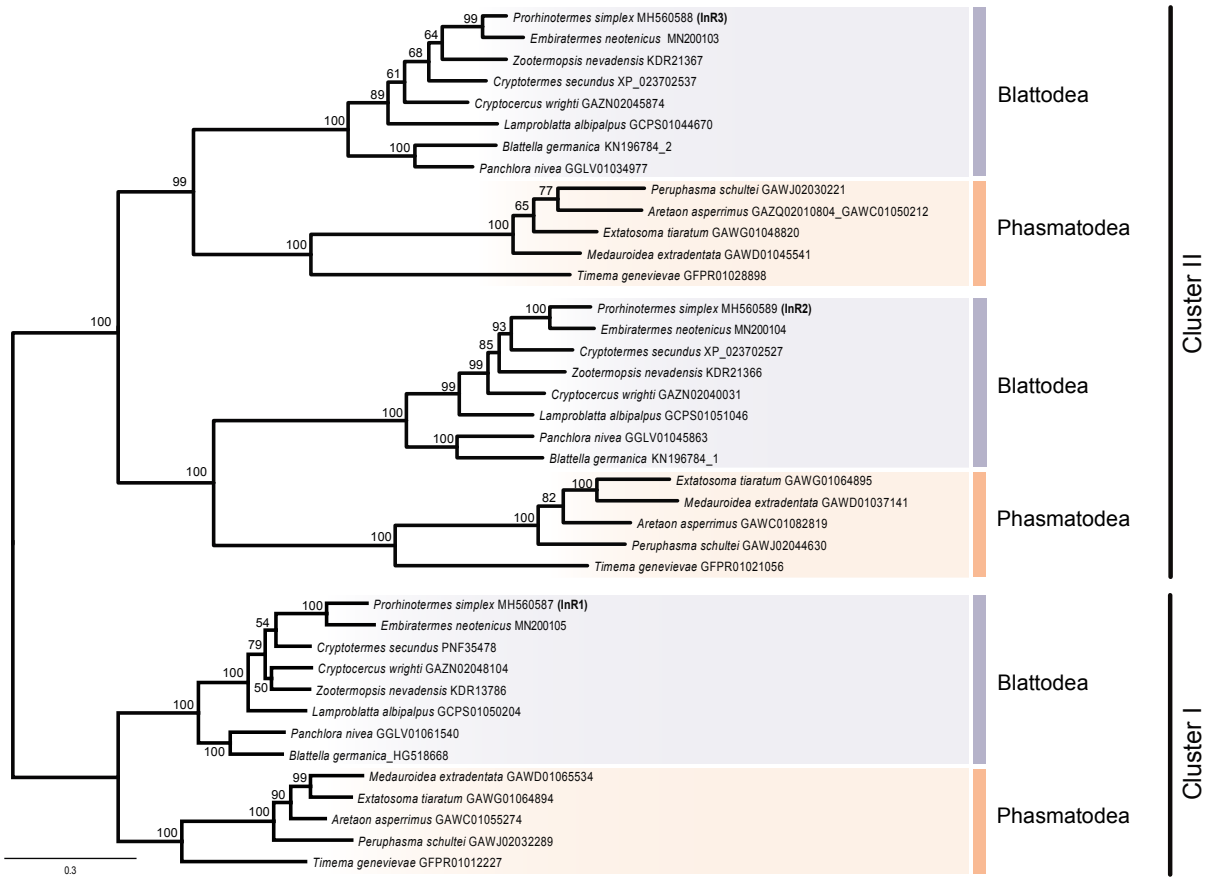

Supplementary Figure 5. Detailed phylogenetic tree of insulin receptor gene sequences identified in eight species of Blattodea and five species of Phasmatodea. The topology and branching were inferred using RAxML maximum likelihood algorithm with WAG + Γ model (-ln = 44434.953962), the bootstrap values calculated from 500 replicates are shown for nodes represented in more than 50% of trees.

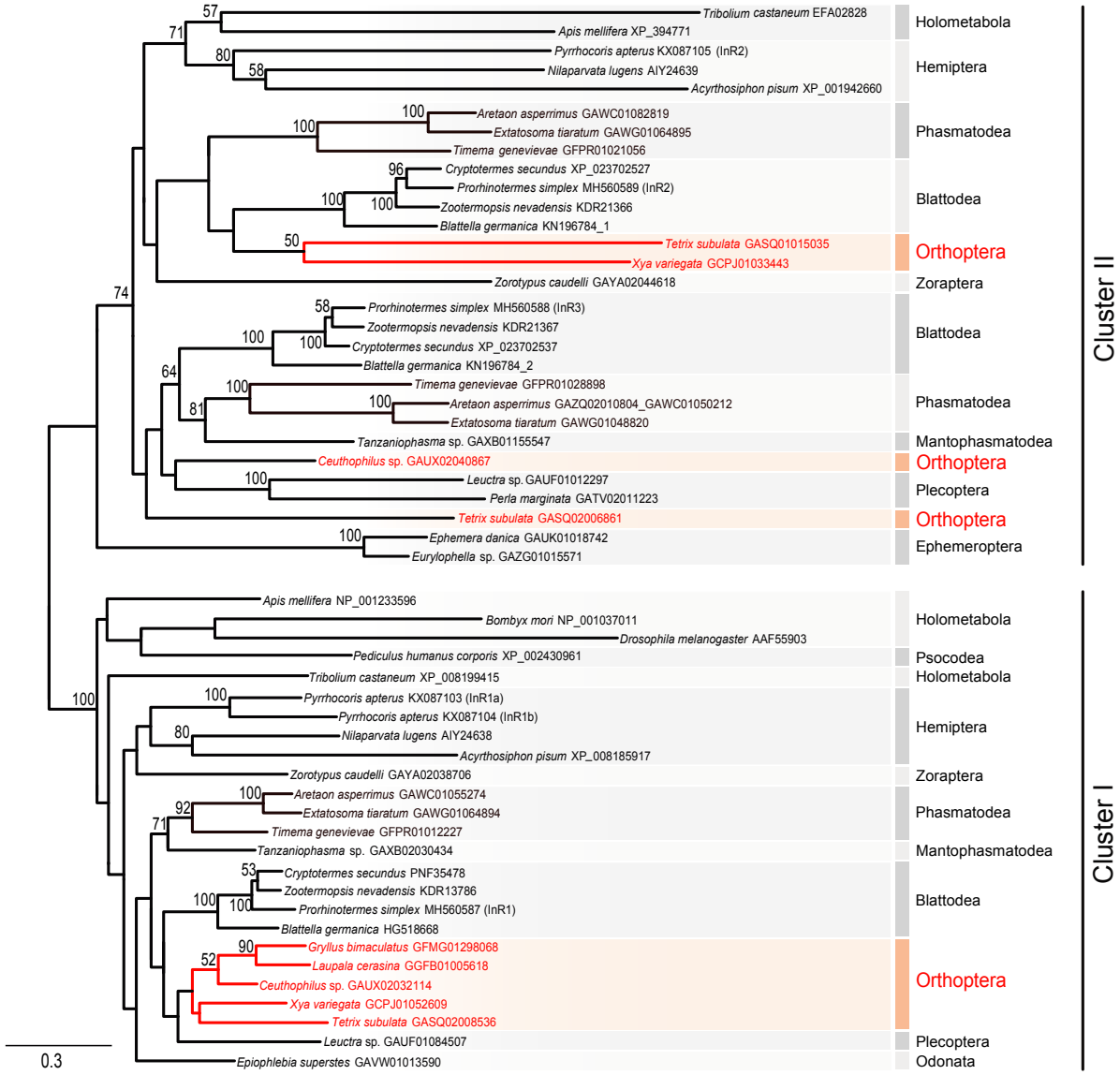

Supplementary Figure 6. Detailed phylogenetic tree of insulin receptor gene sequences identified in five species of Orthoptera and major insect lineages for comparison. Orthopteran representatives are marked in red. The topology and branching were inferred using RAxML maximum likelihood algorithm with WAG + Γ model (-ln = 103575.553052; WAG + Γ model), the bootstrap values calculated from 500 replicates are shown for nodes represented in more than 50% of trees.

Supplementary Figure 7. Detailed phylogenetic tree of insulin receptor gene sequences identified in five species of Orthoptera and major insect lineages for comparison. Orthopteran representatives are marked in red. The topology and branching were inferred using Bayesian inference (WAG + Γ model; chain length = 1 milion; MrBayes).

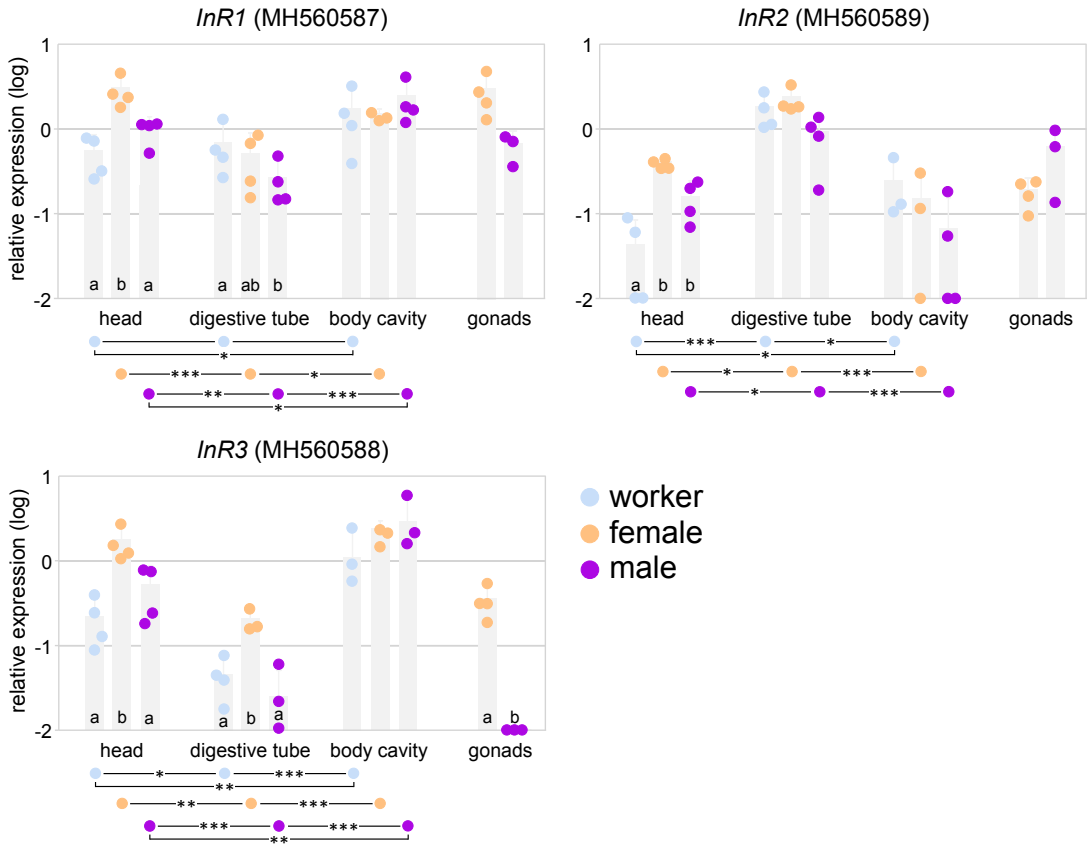

Supplementary Figure 8. Expression pattern of three *InRs* in somatic tissues and gonads of sterile workers (pseudergates) and neotenic reproductives of both sexes 10 days after their moult from workers in the termite *Prorhinotermes simplex*. The graphs show qRT-PCR values of the three genes relative to those of the *rp49* reference gene and log-transformed to reduce heteroscedasticity. Bars show means, whiskers standard deviations. The transformed data was subjected to two-way analysis of variance with sex and tissues as factors. Gonads (absent in workers) were compared separately between males and females using a t-test. 1-3 asterisks denote significant expression differences at $p<0.05$, $p<0.01$, and $p<0.001$, respectively, between different tissues of each caste/sex. Columns marked with different letters indicate significant inter-caste or inter-sex expression differences at $p<0.05$ for individual tissues.

For all three *InRs*, the analyses were evaluated as highly significant, especially due to the significant contribution of the tissues to the total variance ($p<10^{-4}$ for all three *InRs*) and the interaction effects ($p<7\times10^{-3}$ for all three *InRs*). The contribution of caste was retrieved as highly significant for *InR3* ($p<10^{-4}$), while being marginally non-significant for *InR2* ($p=0.056$) and non-significant for *InR1* ($p=0.12$). Post-hoc comparison highlighted several trends in *InRs* expression among tissues. First, *InR2* is highly upregulated in the digestive tube of all castes, while the other two *InRs* show an opposite pattern, having the smallest expression in the digestive tube, except for workers and *InR1*. This points to an eventual differential role of the *InRs* in the nutrient sensing. Last but not least, all *InRs* had larger expression in the body cavity than in heads in workers and in males (except for *InR2* in males).

Intercaste differences included significantly higher expressions of all three InRs in heads of females (*InR2* also in males) when compared to workers. The same applied for *InR3* and the digestive tube. Separate evaluation of *InR* expression in gonads of reproductives revealed a dramatic difference in *InR3* expression in favor of female gonads when compared to very low values in male testes, making the *InR3* a female biased gene in all tissues but body cavity. *InR1* had high expression values and *InR2* moderate expression in gonads of both sexes without striking inter-sex differences.

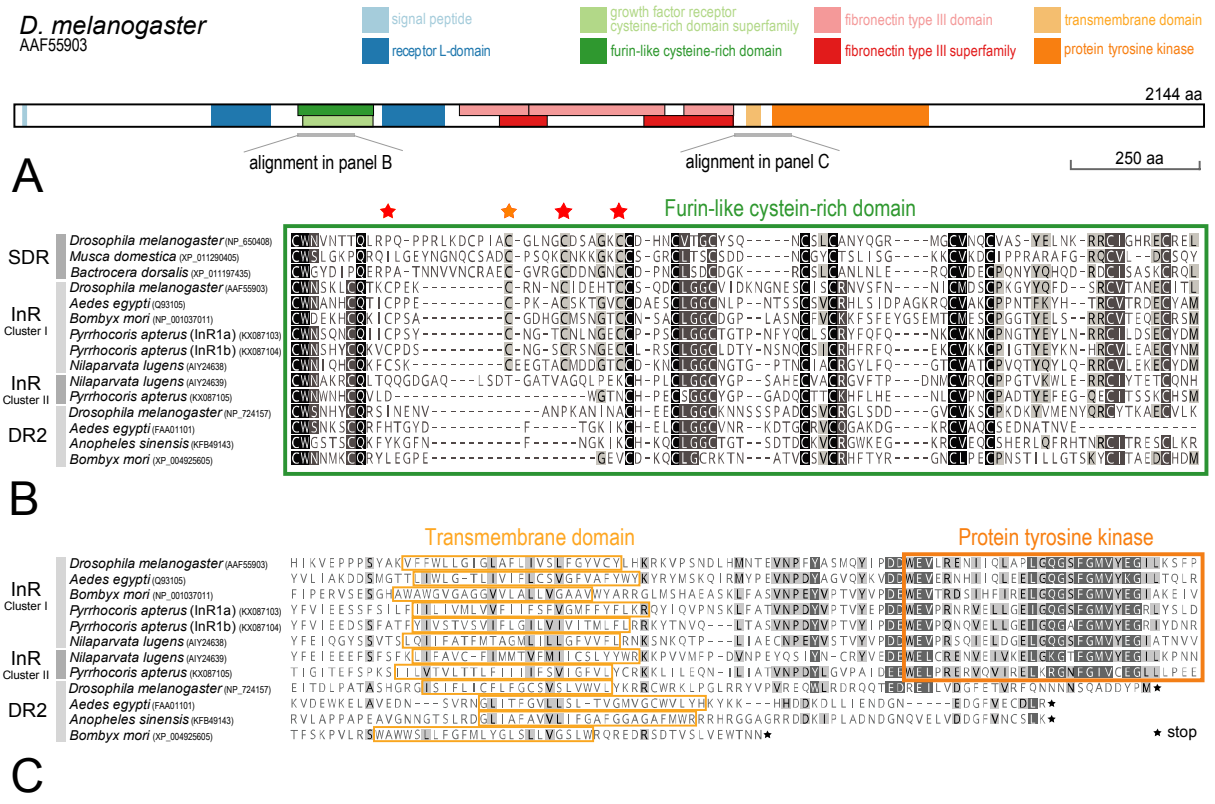

Supplementary Figure 9. Protein domains and alignments of InRs and decoys of insulin receptors in selected insect taxa. **A.** Protein domains recognized in a typical InR (*D. melanogaster*). **B.** Detail of protein alignment covering Furin-like cystein-rich domain. Red asterisks indicate cysteine residues identified as InR1-specific by Xu et al. (2015), the orange asterisk highlights additional residue unique to Cluster I InRs and SDRs. **C.** Detail of protein alignment covering transmembrane domain identified in InRs and DR2s. Small black asterisk indicates C terminus in DR2 proteins. N-terminal part of protein tyrosine kinase domain is highlighted in InRs.

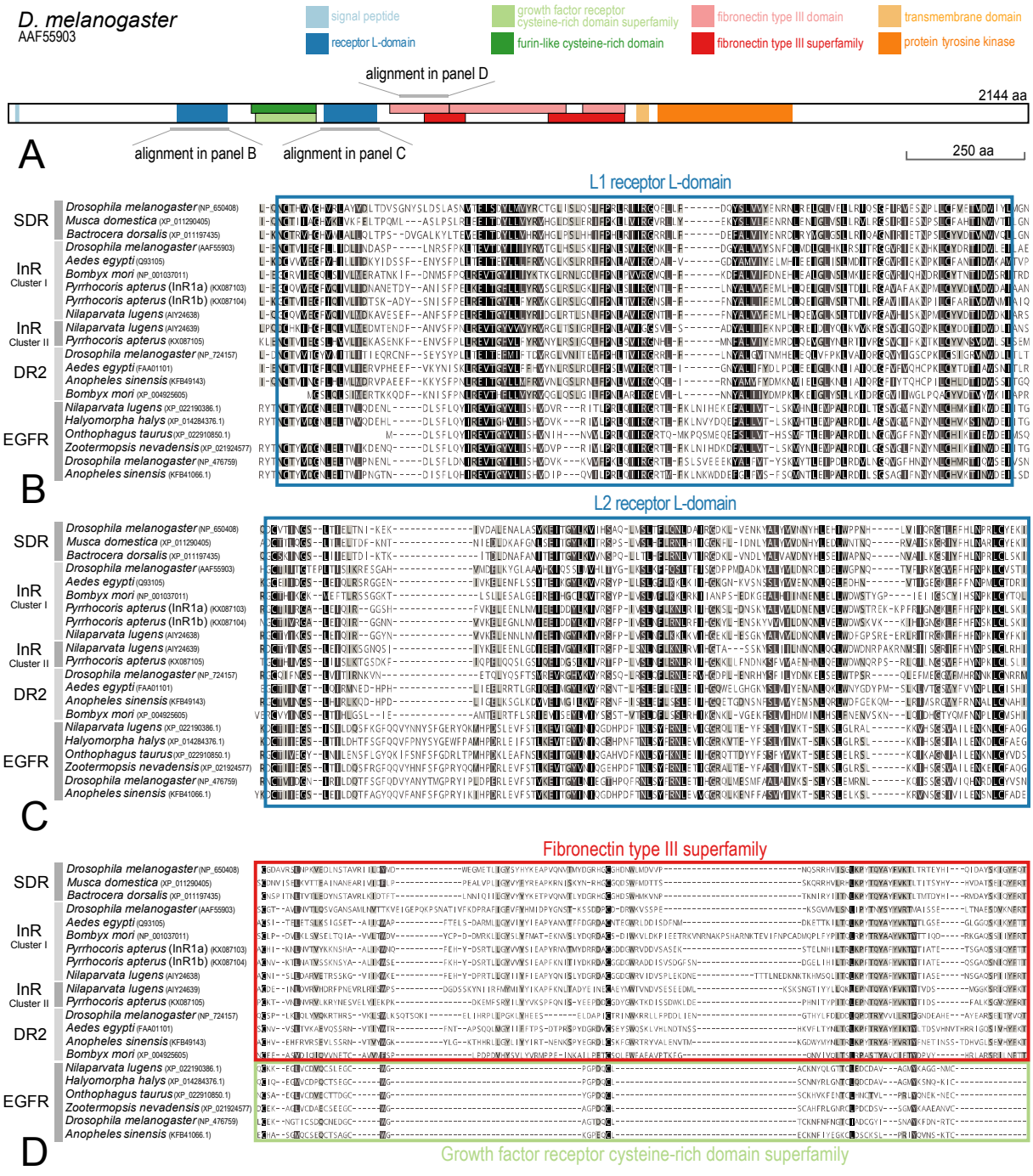

Supplementary Figure 10. Protein domains and alignments of InRs and decoys of insulin receptors in selected insect taxa compared to epidermal growth factor receptor (EGFR). **A.** Protein domains recognized in a typical InR (*D. melanogaster*). **B.** L1 receptor L-domain. **C.** L2 receptor L-domain. **D.** Fibronectin type III superfamily in InRs and Growth factor receptor cysteine-rich domain superfamily in EGFRs.

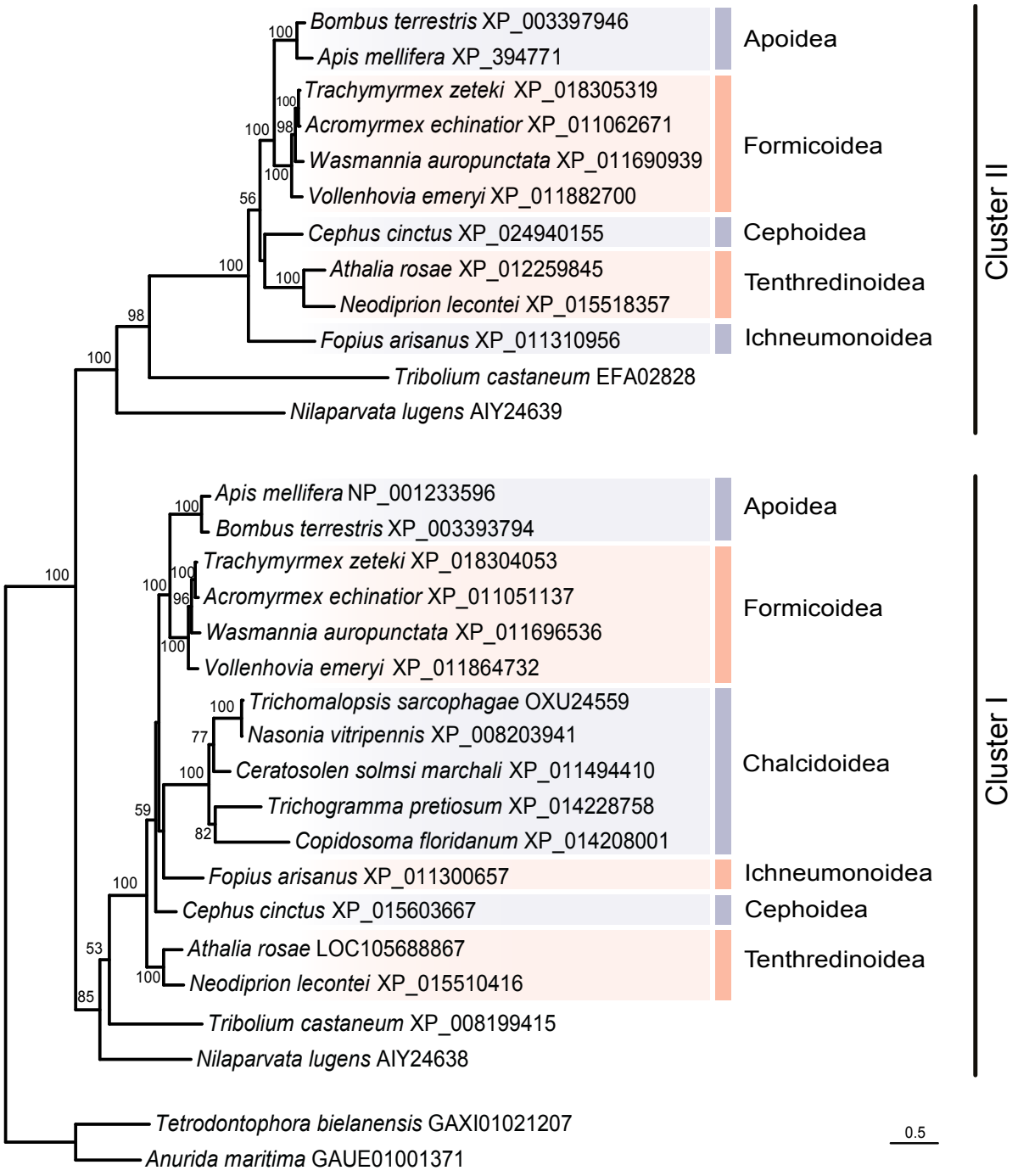

Supplementary Figure 11. Detailed phylogenetic tree of insulin receptor gene sequences identified in 15 species of Hymenoptera. The topology and branching were inferred using RAxML maximum likelihood algorithm with WAG + Γ model (-ln = 59986.190587; WAG + Γ model), the bootstrap values calculated from 1000 replicates are shown for nodes represented in more than 50% of trees.

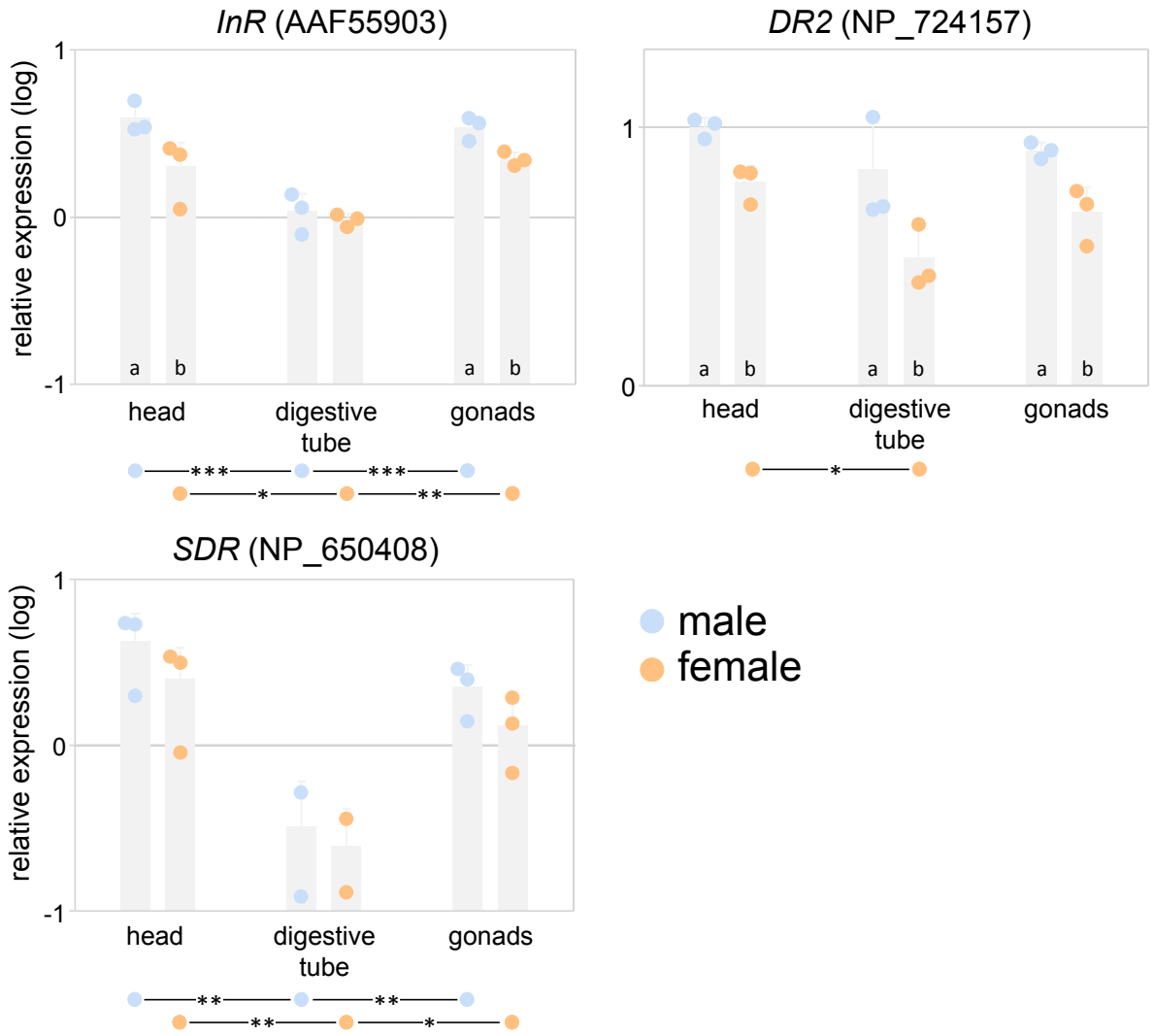

Supplementary Figure 12. Expression pattern of *InR* and decoy receptor genes *SDR* and *DR2* in somatic tissues and gonads of adult fruit flies *Drosophila melanogaster*. The graphs show qRT-PCR values of the three genes relative to those of the control reference gene *rp49* and log-transformed to reduce heteroscedasticity. Bars show means, whiskers standard deviations. The transformed data was subjected to two-way analysis of variance with sex and tissues as factors. 1-3 asterisks denote significant expression differences at probability values $p<0.05$, $p<0.01$, and $p<0.001$, respectively, between different tissues of each sex. Columns marked with different letters indicate significant inter-sex differences at $p<0.05$ for individual tissues.

All three genes are expressed in all studied tissues of both sexes and have similar expression patterns with low values in the digestive tube and higher expression in the head and gonads. Another general trend is a male-biased expression, most pronounced in the case of *DR2*. Two-way analysis of variance with sex and tissue as considered factors revealed that for *InR* and *SDR*, the tissue differences are the main driving force for the total significance of the tests ($p<10^{-4}$ and $p<5\times10^{-4}$, respectively), while the inter-sex differences are of secondary importance ($p<4\times10^{-3}$ and $p=0.21$, interaction $p=0.15$ and 0.84, respectively). By contrast, the male-female difference was evaluated as the main contributor to the overall significance in *DR2* ($p<4\times10^{-4}$), compared to the tissues ($p<10^{-2}$, interaction $p=0.7$).

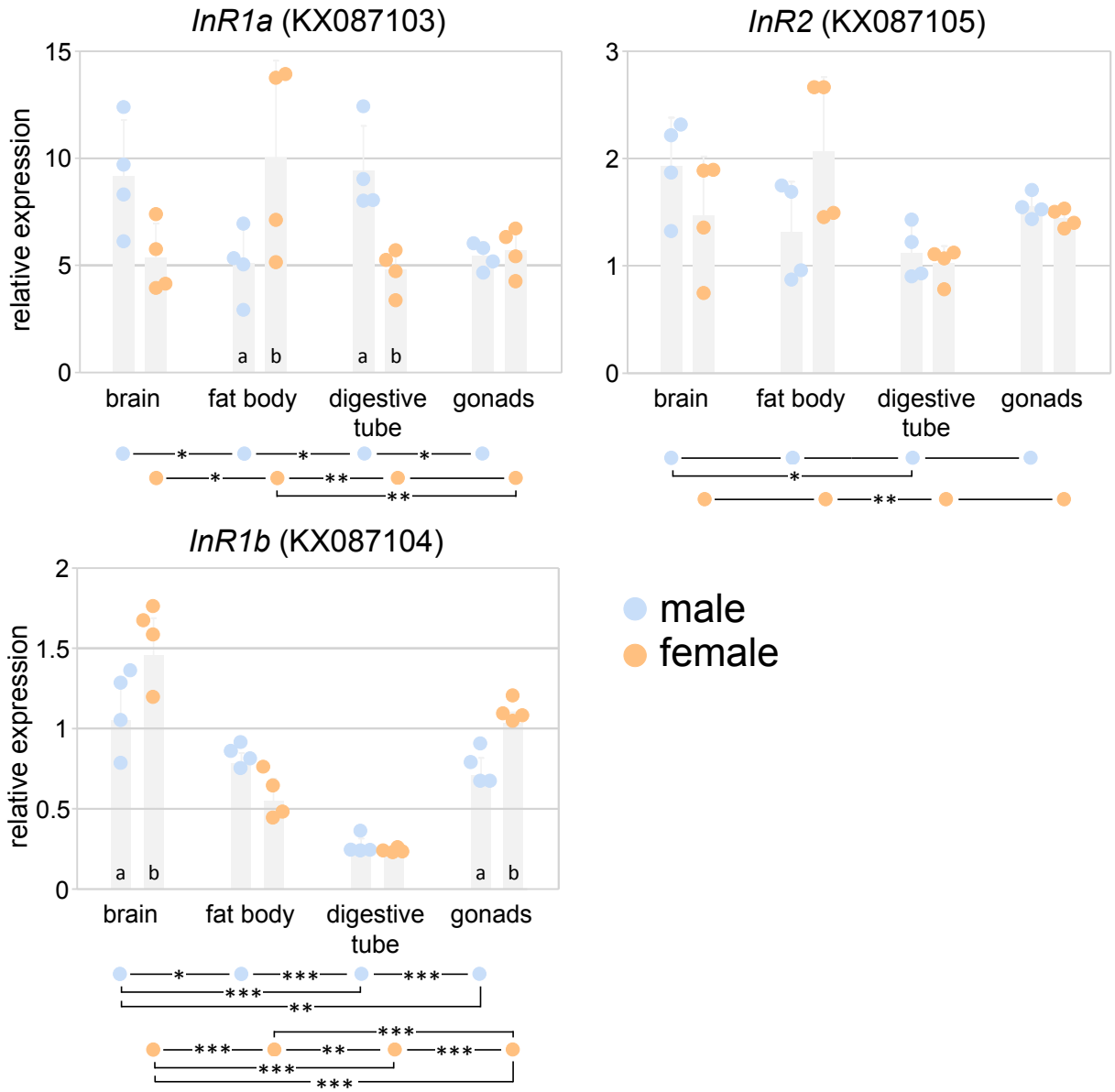

Supplementary Figure 13. Expression pattern of three *InRs* in somatic tissues and gonads of adult linden bugs *Pyrrhocoris apterus*. The graphs show qRT-PCR values of the three genes relative to those of the control reference gene *rp49*. Bars show means, whiskers standard deviations. The data was subjected to two-way analysis of variance with sex and tissues as factors. 1-3 asterisks denote significant expression differences at $p<0.05$, $p<0.01$, and $p<0.001$, respectively, between different tissues of each sex. Columns marked with different letters indicate significant inter-sex differences at $p<0.05$ for individual tissues.

Both *InR1a* and *InR1b* genes are expressed in adults of both sexes, just as it is the case for the Cluster II *InR* (KX087105, hereafter *InR2*). *InR1a* shows the highest transcript abundances in all tissues of both sexes, while *InR1b* the lowest. Expression patterns for all three genes are tissue-specific, the most pronounced differences are observed for *InR1b*, which show a downregulation in the digestive tube. Some tissues also show a significant effect of sex on the *InR* expression.

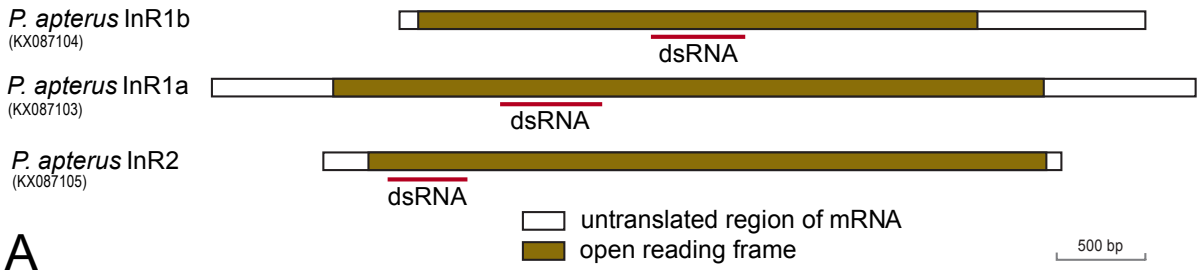

A

	InR2	InR1a	InR1b
dsRNA InR2	100%	50.6%	49.4%
dsRNA InR1a	50.9%	100%	76.0%
dsRNA InR1b	44.9%	75.4%	100%

B

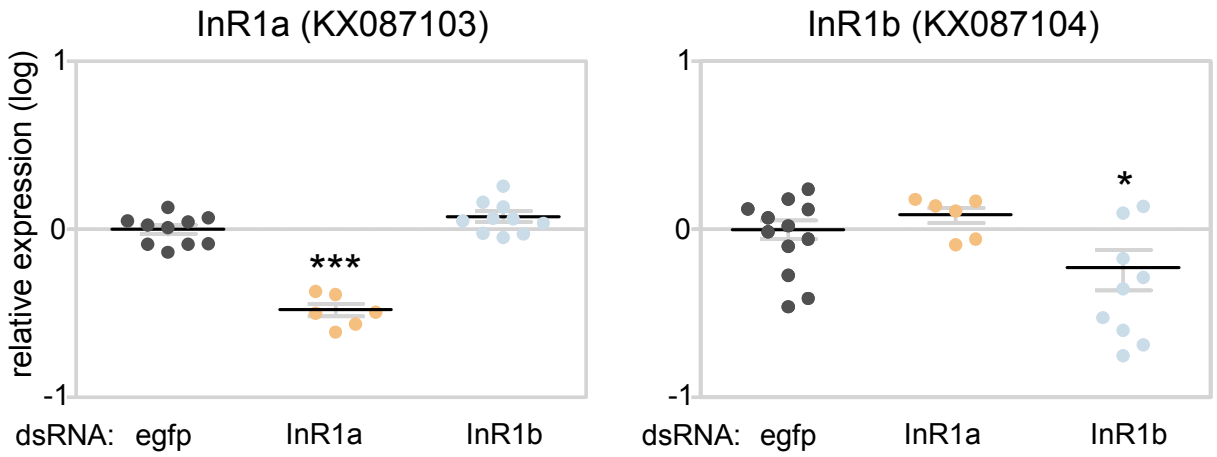

C

Supplementary Figure 14. *Pyrrhocoris apterus InR* transcripts, design of dsRNA and RNAi efficiencies. **A**. *P. apterus InR* transcripts with highlighted open reading frames and positions, for which gene-specific dsRNAs were designed. **B.** Sequence similarity between dsRNA and the corresponding regions in paralogous transcripts agrees with the close relationship between *InR1a* and *InR1b*. **C.** Expression levels (mean±SD) of *InRs1a* (left) and *InR1b* (right) indicate gene-specific targeting in heads of the fourth instar larvae after injection of *egfp* (control), *InR1a* or *InR1b* dsRNA. 1-3 asterisks denote significant differences at $p<0.05$, $p<0.01$, and $p<0.001$, respectively, in expression levels resulting from one-way ANOVA followed with Dunnett posthoc test (*egfp* set as control) on log-transformed data.

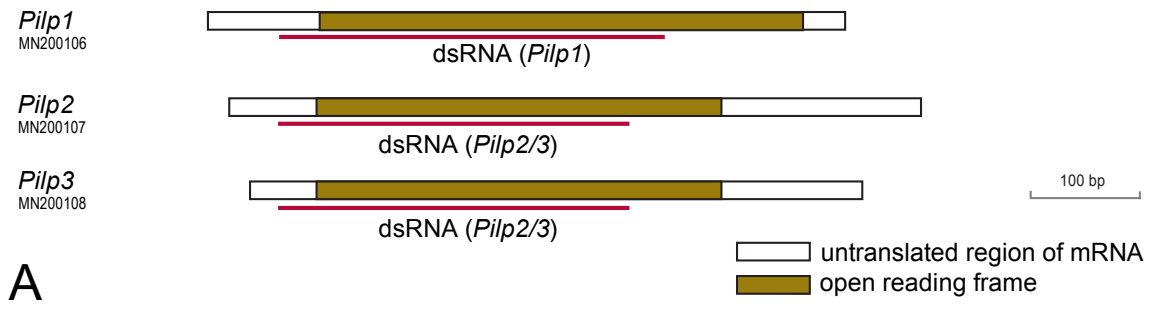

A

B

	Pilp1	Pilp2	Pilp3
dsRNA *Pilp1*	100%	41.5%	43.4%
dsRNA *Pilp2/3*	38.1%	100%	88.9%

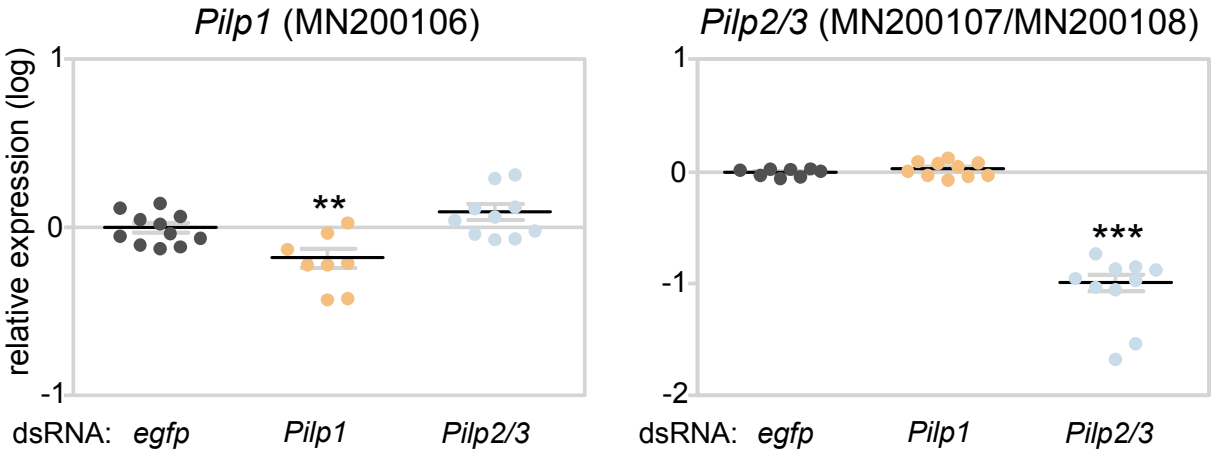

C

Supplementary Figure 15. *Pyrrhocoris apterus insulin-like peptide* (*Pilp*) genes. **A**. *Pilp* transcripts with highlighted open reading frames and positions, for which dsRNAs were designed. **B.** Sequence similarity between dsRNA and the corresponding region in paralogous transcripts agrees with the close relationship between *Pilp2* and *Pilp3*. **C.** Expression levels of *Pilp1* (left graph) and *Pilp2+3* (right graph) in heads of the fourth instar larvae after injection of *egfp* (control), *Pilp1* or *Pilp2+3* dsRNA. 1-3 asterisks denote significant differences at $p<0.05$, $p<0.01$, and $p<0.001$, respectively, in expression levels resulting from one-way ANOVA followed with Dunnett posthoc test (*egfp* set as control) on log-transformed data.

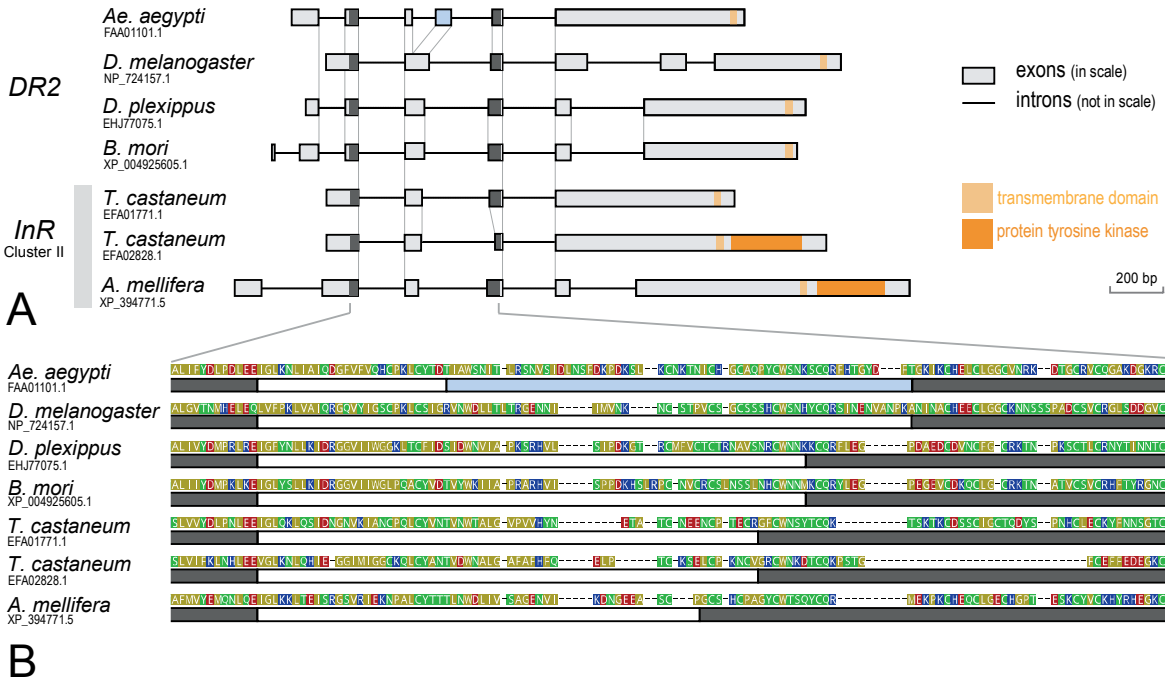

Supplementary Figure 16. Gene structures of two *Tribolium castaneum InR* paralogs identified in the Cluster II compared to representative *DR2* genes and Cluster II *InR* of *Apis mellifera*. **A.** Schematic depiction of exon (boxes) and intron (dotted lines) structure and homologous intron-exon boundaries (gray vertical lines). White, dark grey and blue color in exons correspond to exon coding in panel B. Regions coding for protein tyrosine kinase (dark orange) and transmembrane domain (light orange) are highlighted. **B.** Detail of amino acid sequence alignment with exons indicated as color coded boxes under each sequence.

Supplementary Materials and Methods

Expression of *D. melanogaster InR*, *DR2* and *SDR*

White eye (*w1118*) *D. melanogaster* strain flies were grown on standard corn meal diet at 25 °C. Five days after adult eclosion male and female flies were CO_2-anesthetized and heads, digestive tubes, and gonads were dissected. RNA isolation, reverse transcription and qRT PCR were performed as in *P. apterus* experiments, with *Drosophila*-specific primers (Supplementary table 3, Supplementary Material online). The analysis was performed with three biological replicates, each consisting of pooled tissues from 25 individuals. The quantified transcripts were normalized to the level of the reference gene *rp49* (Bazalova and Dolezel 2017), the results log-transformed to reduce heteroscedasticity and analyzed using two-way ANOVA (tissue and sex as predictors) in GraphPad 5.00.

Expression of *InRs* in the termite *P. simplex* and its caste and tissue specificity

The three *InR* genes identified in *Prorhinotermes simplex* (Rhinotermitidae) were investigated with respect to mRNA levels and eventual caste and tissue-specific expression. For this purpose, we compared their expression in workers (pseudergates), ten-day-old neotenic males and females. The neotenics were obtained from orphaned groups of 100 workers, kept together with 15 soldiers in 9 cm Petri dishes on moistened sand and offered with blocks of spruce wood (permanent darkness, 26°C). In such groups, the workers start to differentiate into neotenics within 10 days. Groups were controlled every 12h, freshly molted neotenics removed and held for ten days in new groups of 50 workers.

Four biological replicates were prepared for each caste and tissue, each of them from pooled tissues of four individuals. Total RNA was isolated using TRI Reagent® (Sigma Aldrich) following the manufacturer's protocol. RNA isolates were treated with RQ1 RNase-Free DNase (Promega) to eliminate contaminant DNA. cDNA template was generated from 0.7 µg of the respective total RNA using the SuperScript III First-Strand Synthesis System (Invitrogen by Life Technologies) and random hexamers. The sequences of specific primers used for amplification are given in supplementary table 3 (Supplementary Material online). qRT-PCR was performed as published earlier (Jirošová et al. 2017). The resulting data was log-transformed to reduce heteroscedasticity and analyzed using two-way ANOVA (tissue and caste/sex as predictors) in GraphPad 5.00.

Expression of *P. apterus InRs* and its sex and tissue specificity

Adults of *Pyrrhocoris apterus* strain Oldrichovec (Pivarciova et al. 2016) were kept in 0.5 liter glass jars on linden seeds and water *ad libitum* in long photoperiod (18 hrs light: 6 hrs dark) at 25 °C. Brain, fat body, digestive tube and gonads were dissected in RNAse-free Ringer's solution from males and females 10 days after adult eclosion, anesthetized by CO_2. Four biological replicates for each tissue and organ were prepared, each from pooled tissues of five individuals. Total RNA was isolated with the Trizol reagent (Invitrogen). After Turbo DNAse (Ambion/ThermoFisher) treatment, 1 µg of total RNA was used for cDNA synthesis using the SuperScript III reverse transcriptase (Invitrogen). Relative transcript levels were measured by quantitative PCR using the qPCR 2x SYBR Master Mix (Top Bio) and the C1000 Thermal Cycler (Bio-Rad). Primers sequences are listed below in supplementary table 3. All measured transcripts were normalized to the level of the reference gene *rp49* (Dolezel et al. 2007). The data was analyzed using two-way ANOVA (tissue and sex as predictors) in GraphPad 5.00.

Identification of *P. apterus* insulin-like peptide (*Pilp*) transcripts

Insect insulin-like peptides (ILPs) from *Drosophila melanogaster* (Dilp1-8), *Bombyx mori* (bombyxin A1-10, B1-12, C1-2, E1, F1, G1) and *Nilaparvata lugens* (NIILP1-4) were used as a query in BLAST searches in our in-house *P. apterus* transcriptomic databases. Candidate hits were validated by reciprocal BLAST searches in NCBI database, protein alignments with insect ILPs, and by position of characteristic Cysteine residues in the preprohormone. The mRNA sequences of three identified *P. apterus insulin-like peptide* (*Pilp*) transcripts were confirmed by PCR and Sanger sequencing.

RNAi-mediated silencing of InRs and Pilps in *P. apterus*

For each *InR*, gene-specific fragment was designed within the open reading frame in regions where stretches of identity between *P. apterus* paralogs where the shortest. In case of the closely related paralogs InR1a and InR1b, specificity of silencing was confirmed by qRT PCR from whole head extracts of 4th instar larvae three days after RNAi. The protocol was identical to tissue-specific quantification, with the exception that RNA was isolated from individual heads and processed separately for RNAi efficiency assessments. Because *Pilp2* and *Pilp3* only differ by several SNPs, both genes were targeted by one common dsRNA. By contrast, *Pilp1* is clearly distinct from *Pilp2+3*. Therefore, one *Pilp1*-targeting and one *Pilp2+3*-targeting fragment were designed within the open reading frame and 5´ untranslated region. The resulting primers are given in supplementary table 4 (Supplementary Material online).

Specific fragments were PCR amplified from head total cDNA by PPP Master Mix (Top Bio, Czech Republic), PCR products were purified by QIAquick PCR Purification Kit (Qiagen), ligated into the pGEM-T Easy vector (Promega) and verified by Sanger sequencing. Templates for dsRNA *in-vitro* synthesis were prepared from pGEM-T Easy clones by PCR using M13 forward and pGEM-RNAi reverse 5'-TAATACGACTCACTATAGGGGACACTATAGAATACT-3' primer replacing SP6 to T7 promoter. Double-stranded RNA was synthesized using MEGAscript T7 Transcription Kit (Ambion/ThermoFisher) following the manufacturer's protocol. dsRNA was then precipitated by adding 0.1 volume of sodium acetate (pH = 5) and 2.5 volume of 100 % ethanol and after spinning and washing it was dissolved in Ringer's solution. As a negative control, 720bp long *egfp* ORF in pEGFP-N1 (Clontech) was digested with SalI and NotI restriction enzymes and subcloned to pBlueScript KS (-) plasmid. T3 promoter in pBlueScript plasmid was replaced by T7 promoter in *in vitro* dsRNA transcription template by using M13F 5'- GTAAAACGACGGCCAGT - 3' and Blue-RNAi-R 5'-AATACGACTCACTATAGGGAACAAAAG - 3' primers.

One-day-old 4th-instar *P. apterus* larvae of both strains were CO_2-anesthetized, attached using a double-sided tape to a small tray and injected ventrolateraly into the abdomen under the stereomicroscope using a micromanipulator (Narishige, Japan) equipped with a borosilicate glass capillary needle. 1 µl of 3-4 µg/µl dsRNA dissolved in Ringer's solution was administered to each larva, which was then transferred to a glass jar supplemented with linden seeds, water, and a folded filter paper. Adult animals were CO_2-anesthetized and scored for wing length. The obtained proportions of long-winged vs. short-winged adult phenotypes were compared with the control treatment using an equivalent of Dunnett test adjusted for proportion data (Zar 1999).

Supplementary Table 1. Insect taxa studied in phylogenetic analyses of InRs and decoy of InRs

higher unit	order	species	acc. number	note
Ametabola	Zygentoma	*Lepisma saccharina*	KX087106	
		Thermobia domestica	GASN02067420	
			GASN02067910	
Palaeoptera	Ephemeroptera	*Ecdyonurus insignis*	GCCL01041136	
			GCCL01030520	
		Ephemera danica	GAUK01018742	AYNC02004105, whole genome shotgun
			GAUK01018485	AYNC02013259, whole genome shotgun
		Eurylophella sp.	GAZG01015571	
Palaeoptera	Odonata	*Cordulegaster boltonii*	GAYO02000575	
		Epiophlebia superstes	GAVW01013590	
		Megaloprepus caerulatus	GEXY01362158	
Polyneoptera	Plecoptera	*Leuctra* sp.	GAUF01084507	
			GAUF01012297	
		Perla marginata	GATV02011223	
Polyneoptera	Zoraptera	*Zorotypus caudelli*	GAYA02038706	
			GAYA02044618	
Polyneoptera	Orthoptera	*Ceuthophilus* sp.	GAUX02040867	used only in detailed analysis (Figures S6, S7)
			GAUX02032114	used only in detailed analysis (Figures S6, S7)
		Gryllus bimaculatus	GFMG01298068	used only in detailed analysis (Figures S6, S7)
		Laupala cerasina	GGFB01005618	used only in detailed analysis (Figures S6, S7)
		Tetrix subulata	GASQ02008536	
			GASQ02006861	
			GASQ01015035	
		Xya variegata	GCPJ01033443	used only in detailed analysis (Figures S6, S7)
			GCPJ01052609	used only in detailed analysis (Figures S6, S7)
Polyneoptera	Mantophasmatodea	*Tanzaniophasma* sp.	GAXB01155547	
			GAXB02030434	
Polyneoptera	Phasmatodea	*Aretaon asperrimus*	GAWC01055274	
			GAWC01082819	
			GAZQ02010804_GAWC01050212	
		Extatosoma tiaratum	GAWG01064894	
			GAWG01048820	
			GAWG01064895	
		Medauroidea extradentata	GAWD01037141	used only in detailed analysis (Figure S5)
			GAWD01045541	used only in detailed analysis (Figure S5)
			GAWD01065534	used only in detailed analysis (Figure S5)
		Peruphasma schultei	GAWJ02030221	used only in detailed analysis (Figure S5)
			GAWJ02044630	used only in detailed analysis (Figure S5)
			GAWJ02032289	used only in detailed analysis (Figure S5)
		Timema genevievae	GFPR01028898	
			GFPR01021056	
			GFPR01012227	
		Timema cristinae		PGFK01000003, PGTA01000614, whole genome shotgun
Polyneoptera	Blattodea	*Blattella germanica*	HG518668	
			KN196784_1	
			KN196784_2	
		Cryptocercus wrighti	GAZN02045874	used only in detailed analysis (Figure S5)
			GAZN02040031	used only in detailed analysis (Figure S5)
			GAZN02048104	used only in detailed analysis (Figure S5)
		Cryptotermes secundus	XP_023702537	
			XP_023702527	
			PNF35478	
		Embiratermes neotenicus	MN200103	used only in detailed analysis (Figure S5)
			MN200104	used only in detailed analysis (Figure S5)
			MN200105	used only in detailed analysis (Figure S5)
		Lamproblatta albipalpus	GCPS01044670	used only in detailed analysis (Figure S5)
			GCPS01051046	used only in detailed analysis (Figure S5)
			GCPS01050204	used only in detailed analysis (Figure S5)
		Panchlora nivea	GGLV01034977	used only in detailed analysis (Figure S5)
			GGLV01045863	used only in detailed analysis (Figure S5)
			GGLV01061540	used only in detailed analysis (Figure S5)
		Prorhinotermes simplex	MH560589	InR2 in this study
			MH560588	InR3 in this study
			MH560587	InR1 in this study
		Zootermopsis nevadensis	KDR13786	
			KDR21367	
			KDR21366	
Paraneoptera	Thysanoptera	*Frankliniella occidentalis*	XP_026277828	
		Phlaeothripidae gen. sp.	GCYQ01040907	
Paraneoptera	Sternorrhyncha	*Acyrthosiphon pisum*	XP_001942660	
			XP_008185917	
		Adelges tsugae	GBJX01018946	
			GBJX01005109	
		Aphis citricidus	ARD07922	
			ARD07921	
		Bemisia tabaci	XP_018897134	
			GEZK01059603	
		Daktulosphaira vitifoliae	GDEB01025952	
			GDEB01020876	
		Diaphorina citri	XP_008479213	
			GACJ01002847	
		Diuraphis noxia	XP_015363980	
			XP_015375915	

Supplementary Table 1, *continued*

higher unit	order	species	acc. number	note
Paraneoptera	Sternorrhyncha	*Myzus persicae*	XP_022180848	
			XP_022180095	
		Pachypsylla venusta	GAOP01019620	
			GAOP01060619+21	
		Phenacoccus solenopsis	GGIT01015335	
			GGIT01003183	
Paraneoptera	Auchenorrhyncha	*Campylenchia latipes*	GCWI01051784	
		Clastoptera arizonana	GEDC01010167	
			GEDC01006489	
		Cuerna arida	GECZ01003109	
		Diceroprocta seminicta	GGPH01050080	
			GGPH01129260	
		Euscelidius variegatus	GFTU01002760	
			GFTU01002463	
			GFTU01007873	
			GFTU01003387	
			GFTU01001093	
		Graminella nigrifrons	GAQX01001711	
			GAQX01006206	
			GAQX01002061	
		Graphocephala atropunctata	GEBQ01020846_01005496	
			GEBQ01031456	
		Homalodisca liturata	GECU01004804	
			GECU01010637	
		Homalodisca vitripennis	HVIT002229_PA	
			HVIT005314_PA	
			HVIT005312_PA	
			HVIT016189_PA	
		Mapuchea sp.	GCXN01044447_1045662	
			GCXN01060330	
		Neotibicen dorsatus	GCYV01053567	
			GCYV01046097	
		Nilaparvata lugens	AIY24639	
			AIY24638	
Paraneoptera	Heteroptera	*Alydus pilosus*	GCVZ01036674	
		Anasa tristis	GCWG01047286	
		Aquarius paludum	INR2	sequences available in Armisén et al. (2018)
			INR1	sequences available in Armisén et al. (2018)
			INR1-like	sequences available in Armisén et al. (2018)
		Cimex lectularius	XP_014256336	
			XP_014242611	
		Gerris buenoi	INR2	JHBY02017739; JHBY02040390 whole genome shotgun
			INR1	JHBY02000552; JHBY02000555; JHBY02000556 whole genome shotgun
			INR1-like	JHBY02104847, whole genome shotgun
		Halyomorpha halys	XP_024217440	
			XP_014273515	
		Hebrus sp.	INR2	sequences available in Armisén et al. (2018)
			INR1	sequences available in Armisén et al. (2018)
			INR1-like	sequences available in Armisén et al. (2018)
		Hydrometra cumata	INR2	sequences available in Armisén et al. (2018)
			INR1	sequences available in Armisén et al. (2018)
			INR1-like	sequences available in Armisén et al. (2018)
		Jadera haematoloma	AVT56265	
			AVT56264	
		Largus californicus	GCXR01064717	
			GCXX01059075	
		Limnoporus dissortis	INR2	sequences available in Armisén et al. (2018)
			INR1	sequences available in Armisén et al. (2018)
			INR1-like	sequences available in Armisén et al. (2018)
		Lygus hesperus	JAG02168	
			JAG20929	
		Mesovelia furcata	INR2	sequences available in Armisén et al. (2018)
			INR1	sequences available in Armisén et al. (2018)
			INR1-like	sequences available in Armisén et al. (2018)
		Microvelia longipes	INR2	sequences available in Armisén et al. (2018)
			INR1	sequences available in Armisén et al. (2018)
			INR1-like	sequences available in Armisén et al. (2018)
		Oncopeltus fasciatus	AVT56270	
		Pagasa sp.	GCXU01030579	
			GCXU01024823	
		Podisus maculiventris	GFUB01178628	
			GFUB01166485	
		Pyrrhocoris apterus	KX087104	InR1b in this study
			KX087103	InR1a in this study
			KX087105	InR2 in this study
		Rhagovelia antilleana	INR2	sequences available in Armisén et al. (2018)
			INR1	sequences available in Armisén et al. (2018)
			INR1-like	sequences available in Armisén et al. (2018)
		Rhodnius prolixus	GECK01011918	
			GECK01019799	

Supplementary Table 1, *continued*

higher unit	order	species	acc. number	note
Paraneoptera	Psocodea	*Badonnelia titei*	GDFG01033096	
		Geomydoecus ewingi	GCXD01012496	
		Lachesilla contraforcepeta	GCWJ01026792	
		Liposcelis bostrychophila	GAYV01001422	
		Pediculus humanus corporis	XM_002430916	
Holometabola	Hymenoptera	*Acromyrmex echinatior*	XP_011062671	used only in detailed analysis (Figure S8)
			XP_011051137	used only in detailed analysis (Figure S8)
		Apis mellifera	NP_001233596	
			XP_394771	
		Athalia rosae	LOC105688867	
			XP_012259845	
		Bombus terrestris	XP_003393794	used only in detailed analysis (Figure S8)
			XP_003397946	used only in detailed analysis (Figure S8)
		Cephus cinctus	XP_024940155	
			XP_015603667	
		Ceratosolen solmsi marchali	XP_011494410	used only in detailed analysis (Figure S8)
		Copidosoma floridanum	XP_014208001	used only in detailed analysis (Figure S8)
		Fopius arisanus	XP_011300657	
			XP_011310956	
		Nasonia vitripennis	XP_008203941	
		Neodiprion lecontei	XP_015518357	used only in detailed analysis (Figure S8)
			XP_015510416	used only in detailed analysis (Figure S8)
		Solenopsis invicta	JF304723	
			JF304722	
		Trachymyrmex zeteki	XP_018305319	used only in detailed analysis (Figure S8)
			XP_018304053	used only in detailed analysis (Figure S8)
		Trichogramma pretiosum	XP_014228758	used only in detailed analysis (Figure S8)
		Trichomalopsis sarcophagae	OXU24559	used only in detailed analysis (Figure S8)
		Vollenhovia emeryi	XP_011882700	used only in detailed analysis (Figure S8)
			XP_011864732	used only in detailed analysis (Figure S8)
		Wasmannia auropunctata	XP_011696536	used only in detailed analysis (Figure S8)
			XP_011690939	used only in detailed analysis (Figure S8)
Holometabola	Coleoptera	*Dendroctonus ponderosae*	XP_019755840	
			XP_019765260	
		Leptinotarsa decemlineata	XP_023030119	
			XP_023021383	
		Pogonus chalceus	JU427775	
			JU418048	
		Tribolium castaneum	EFA02828	
			XP_008199415	
			EFA01771	
Holometabola	Raphidioptera	*Xanthostigma xanthostigma*	GAUI02048109	
			GAUI02044701	
Holometabola	Neuroptera	*Chrysopa pallens*	AVK43098	
			AVK43099	
Holometabola	Lepidoptera	*Bombyx mori*	NP_001037011	
			XP_004925605	DR2
		Danaus plexippus	EHJ65074	
			EHJ77075	DR2
		Plutella xylostella	XP_011567916	
			XP_011567028	DR2
Holometabola	Trichoptera	*Annulipalpia* sp.	GATX01009258_01085969	
			GATX01005845	DR2
			GATX01012065	DR2
		Platycentropus radiatus	GASS02029169	
			GASS02028789	DR2
Holometabola	Siphonaptera	*Ceratophyllus gallinae*	GAWK02019316	
		Ctenocephalides felis	XP_026475386	
Holometabola	Mecoptera	*Boreus hyemalis*	GAYK01004971	
			GAYK01108088	DR2
Holometabola	Diptera	*Aedes aegypti*	Q93105	
			FAA01101	DR2
		Anopheles sinensis	KFB49958	
			KFB49143	DR2
		Ceratitis capitata	XP_004518075	
			XP_004519681	SDR
			XP_004527212	DR2
		Clunio marinus	CRL08130	
			CRL06839	DR2
		Drosophila melanogaster	AAF55903	
			NP_650408	SDR
			NP_724157	DR2
		Liogma simplicicornis	GEMK01036784	
			GEMK01029352	DR2
		Musca domestica	XP_005178583	
			XP_011290405	SDR
			XP_011291787	DR2
		Nyssomyia neivai	JAV06640	
		Sarcophaga peregrina	GGEP01027089	
			GGEP01012125	SDR
			GGEP01039589	DR2

Supplementary Table 2. Accession numbers of genomic sequences used for gene structure analysis

higher unit	order	species	acc. number	note
Crustacea	Cladocera	*Daphnia pulex*	FLTH02000001.1	Cluster I
Palaeoptera	Ephemeroptera	*Ephemera danica*	AYNC02013259.1	Cluster I
			KZ497776.1	Cluster II
Polyneoptera	Phasmatodea	*Timema cristinae*	CM009478.1	Cluster I
			PGTA01000614	Cluster II
Polyneoptera	Blattodea	*Prorhinotermes simplex*	MH560587	Cluster I (InR1 in this study)
			MH560588	Cluster II (InR2 + InR3 in this study)
Paraneoptera	Heteroptera	*Gerris buenoi*	KZ651042.1	Cluster I (InR1)
			JHBY02104847.1	Cluster I (InR1-like)
			KZ651484.1 + KZ651190.1	Cluster II
		Pyrrhocoris apterus	MN987938	Cluster I (InR1a in this study)
			MN987939	Cluster I (InR1b in this study)
			MN987940	Cluster II (InR2 in this study)
Paraneoptera	Psocodea	*Pediculus humanus corporis*	DS235841.1	Cluster I
Holometabola	Hymenoptera	*Apis mellifera*	NC_037639.1	Cluster I
			NC_037646.1	Cluster II
Holometabola	Lepidoptera	*Bombyx mori*	NW_004582016.1	Cluster I
			NW_004581734.1	Cluster II (DR2)
Holometabola	Diptera	*Aedes aegypti*	NC_035108.1	Cluster II (DR2)
		Drosophila melanogaster	NT_033777.3	Cluster I (InR, c. map: 93E4-93E9, CG18402)
			NT_033777.3	Cluster I (SDR, c. map: 88D7, CG3837)
			NT_033779.5	Cluster II (DR2)

Supplementary Table 3. Primers used for qRT PCR analyses of InRs and decoy of InR

species	gene	accession number	forward primer (5´-3´)	reverse primers (5´-3´)
Prorhinotermes simplex	*InR1*	MH560587	CTGCCAGGCTTCACAGACCT	ATGCGTCCCGTCCATCATAC
	InR2	MH560589	CCCGCCATGCTGAGATTTTTG	AGCCAGACTCACATATTCAGGATT
	InR3	MH560588	TTCGCCGTATGTTGCTGATG	TCTCAGGAGCCATCCATCGT
	rp49	GASE02006626	CTGGTGCATAACGTGAAGGAACT	CAGGCGAGCATTAGCATTTGTA
Pyrrhocoris apterus	*InR1a*	KX087103	TGTCAATGTACAGGCAGCAGAT	GCTGACCTTGAGAAACAACACC
	InR1b	KX087104	TCCTGATGAGTGGGAAGTAC	CTGCACAGGGTTTCACTAAAGAG
	InR2	KX087105	GCCGAGTCCGAACCTGATGG	CTGCCCGAGTTCTAGACCCTGTAT
	rp49	GDFI01014277	CCGATATGTAAAACTGAGGAGAAAC	GGAGCATGTGCCTGGTCTTTT
Drosophila melanogaster	*InR*	CG18402; AAF55903	AAGTCCTGCGTTACGTCATC	TCTCGCCGAAGACCTATGAT
	SDR	CG3837; NP_650408	CATGACAACTGGCTGATGG	CGTCTGGAAGTAGCCGATTT
	DR2	CG10702; NP_724157	GATGTGATGACGCCCTACAT	CACCCAAACAGGAAGCAGAT
	rp49	NM_170460	GATATGCTAAGCTGTCGCACA	CACCAGGAACTTCTTGAATCC

Supplementary Table 4. Primers used for dsRNA templates in *P. apterus*

gene	accession number	forward primer (5´-3´)	reverse primers (5´-3´)
InR1a	KX087103	CTGCTAGAATGCCCTACCAA	GCATGCAACTTTGTCTCCAT
InR1b	KX087104	GGTAGAATTGTGGGATTGGA	AGCCCCACTTTGTTCAGTAG
InR2	KX087105	TTCAGCCTACTACCACAAGAC	GTTAGACGACGGACAGTTACA
Pilp1	MN200106	ACTTGTTTCAAGGGATCTCCGT	ACCTGTTGTAACTTTCAGTTTCAAGT
Pilp2/3	MN200107/MN200108	AGAAGGACTCATTTGAGCAGCA	CCTGTACTCGAGGATTGACAGG

Supplementary references

Bazalova O, Dolezel D. 2017. Daily activity of the housefly, *Musca domestica*, is influenced by temperature independent of 3' UTR period gene splicing. *G3* 7:2637–2649.

Dolezel D, Sauman I, Kostal V, Hodkova M. 2007. Photoperiodic and food signals control expression pattern of the clock gene, period, in the linden bug, *Pyrrhocoris apterus*. *J Biol Rhythms* 22:335-342.

Jirošová A, Jančařík A, Menezes RC, Bazalová O, Dolejšová K, Vogel H, Jedlička P, Buček A, Brabcová J, Majer P, Hanus R, Svatoš A. 2017. Co-option of the sphingolipid metabolism for the production of nitroalkene defensive chemicals in termite soldiers. *Insect Biochem Mol Biol* 82:52–61.

Pivarciova L, Vaneckova H, Provaznik J, Wu BC, Pivarci M, Peckova O, Bazalova O, Cada S, Kment P, Kotwica-Rolinska J, Dolezel D. 2016. Unexpected geographic variability of the free running period in the linden bug *Pyrrhocoris apterus*. *J Biol Rhythms* 31:568–576.

Zar JH. 1999. Biostatistical analysis. New Jersey: Prentice Hall, Inc.